# Modeling mechanochemical coupling in cell polarity maintenance

Ondrej Maxian

February 17, 2024

Cell polarity is essential for many aspects of organismal development and physiology, including stem cell dynamics, directional cell migration, and asymmetric cell division [6, 10, 12, 18]. On a large scale, a cell's polarity state is encoded by asymmetric distributions of protein molecules, which are shaped by smaller-scale processes like binding, diffusion, and active transport. The key group of proteins involved in this process are the so-called PAR proteins, which are highly conserved across the metazoa, and are typically distributed asymmetrically during cell division [14, 17] in the presence of actomyosin-mediated contractile flows [21].

The one-cell *C. elegans* embryo is one of the premier model systems for polarization in eukaryotic cells. In this system, polarity is encoded by the distribution of two distinct groups of polarity proteins: anterior PARs (aPARs), which include PAR-3, PAR-6/PKC-3, and CDC-42, and posterior PARs (pPARs), which include PAR-2, PAR-1, LGL-1, and CHIN-1 [17]. Wild-type embryos polarize in two distinct phases termed "establishment" and "maintenance" [3]. In establishment phase, a local sperm cue at the anterior pole acts to load PAR-2 onto the membrane, while at the same time promoting strong anterior-directed actomyosin flows [7]. These cues, together with the mutual inhibition of the aPAR and pPAR domain, sort the PAR proteins into their respective domains, where they are then maintained during maintenance phase [21, 24].

In the language of dynamical systems, it can therefore be said that the *C. elegans* embryo possesses two stable states: a uniform state, in which all of the proteins are distributed symmetrically throughout the cell, and a polarized state, in which the PAR proteins are sorted into their respective domains. The switch between the two states is then governed by the sperm cue, which drives an advective flow to transform the uniform state to the polarized one [9, 11]. Indeed, recent theoretical and experimental studies showed that the cell operates in a regime where cues are necessary to establish polarity, thus avoiding the potentially chaotic case of spontaneous polarization without cues [11].

This analysis suggests that cue-driven flows are required for polarity establishment, and that flow

patterns PAR proteins. Yet, it has been demonstrated repeatedly that embryos lacking a functional flow during establishment phase still polarize, albeit in a delayed manner, and furthermore find the same boundary position as embryos with a functional establishment-phase flow [27, 26]. The flows in these embryos result from a switch from rho-dependent contractility in establishment phase to CDC-42-dependent contractility in maintenance phase [24]. Still though, absent the cue the PAR proteins are the only agents that could pattern actomyosin flows. Thus, these "maintenance-phase" rescue experiments hint that PAR proteins pattern flows, rather than the other way around. This gets at the general question: what are the design principles by which cells combine the PAR protein circuit with actomyosin to robustly encode a dynamically stable polarity state with a fixed boundary position?

Because of the complexity of the *in vivo* system, a definitive answer to this question is only possible with a combination of experiments and modeling. This fact was recognized early on in the field, and indeed there is no dearth of models in the literature (see [25, 5, 4, 8, 11, 9, 15] for a subset). In early models, *potential* mechanics for polarization were explored, but the relative abundance of experimental data in the last decade can allow us to be more precise. For example, an early model of Tostevin and Howard showed that polarity sorting could occur if actomyosin flows feedback onto the aPAR [25] but not pPAR distribution, but recent experiments have shown that both cortical aPARs and pPARs are transported by myosin [13]. We do not take the harsh view that these early models are incorrect; rather, we view them as missing some fundamental biochemistry that was at the time unknown. Consequently, our goal here is to construct a minimal model based on existing experimental evidence that shows how the combination of aPAR/pPAR mutual inhibition and actomyosin flows generate a stable polarity state with fixed boundary position.

Still working on this introductory part. Once we set up a bistable reaction system, the question becomes how we can move from the uniform to the polarized state. Experiments suggest that there are two intrinsic boundary positions here: one (at about 75% egg length) that occurs in the absence of actomyosin flows, and another (at about 50% egg length) that occurs with actomyosin flows [27]. The second case suggests that flows alter the flux balance between the anterior and posterior domains, thus shifting the boundary positions. Indeed, there is a steady state nonzero flow profile observed during maintenance phase, corresponding to an asymmetry in myosin intensity across the A/P boundary [23].

Two questions arise when we consider this data: first, how is the myosin asymmetry maintained without cues? Second, what "brakes" the contractility, i.e., what stops the anterior cap

2

from contracting off the end of the embryo? The first question can be answered again through experiments and modeling, which have shown that PAR proteins feedback onto myosin dynamics [11, 1]. It remains unclear whether this occurs through pPARs inhibiting myosin (as suggested by [1]) or aPARs recruiting myosin (or inhibiting its dissociation, as suggested in [11]). Modeling work has shown that pPARs *must* inhibit myosin to propagate initially asymmetric protein distributions [15]. Seeing as this hypothesis has been supported experimentally [21, 1], it is the one we use in this work.

Once we set up dynamics in which aPARs and pPARs are mutually bistable, and pPARs inhibit myosin, it is straightforward to see how maintenance phase "rescue" could occur, as the already expanding pPAR domain is then further extended by flow caused from inhibited myosin. But how could this process stop? Previous work [9] proposes a "pinning" of the boundary [20] based on cytoplasmic depletion of PAR-2. As the PAR-2 domain expands, the amount available in the cytoplasm decreases. This changes the local binding/unbinding equilibrium, leading to relative depletion of PAR-2 in the posterior. This levels off myosin inhibition levels, which prevents the build up of strong flows, stalling the boundary.

We propose that this mechanism, while theoretically possible and reproducible in our model, is not the one primarily responsible for stalling the boundary movement. Instead, we postulate that branched actin acts to inhibit contractility in the anterior domain, which prevents myosin from building up and generating stronger flows. We demonstrate one of these two things:

1. The hypercontractile state is stable. We can pin it down with the PAR-2 wave-pinning mechanism. The model predicts decreasing PAR-2 on the posterior in this case, which is supported by our experiments.

2. The hypercontractile state is not stable. While we can reproduce it in the model, there is no way to reconcile the parameters we need to reproduce it with the parameters we need to reproduce the wild-type.

Finally, we use modeling to show that branched actin-mediated inhibition of myosin leads to the experimentally-observed myosin and flow profiles, thus validating our hypothesis.

In Section 3.1, we first rule out the hypothesis that maintenance-phase rescue is driven by spontaneous polarization of myosin, as the flows generated are simply too small to spontaneously polarize the embryo (similar to observations made in establishment phase [22]). We therefore need to incorporate biochemistry to guide the dynamics of myosin. In previous work by some of us [16],

we showed that the maintenance-phase dynamics of PAR-3 are bistable even in the absence of the posterior inhibitor PAR-1. Because of this, it is our hypothesis that PAR-3 provides an anchor for the bistability of the entire system. We utilize this hypothesis in Section 3.2, where we set up a model describing the maintenance phase biochemistry. While this model is capable of amplifying small asymmetries to produce polarized states, the timescale on which this occurs is roughly ten times larger than the duration of maintenance phase, indicating the need for contractility to speed up the process. Therefore, in Section 3.4, we demonstrate how combining our biochemistry and contractility models can reproduce maintenance-phase experimental observations.

# 1    The distinction between establishment and maintenance

(A) Cell cycle progression controls a regime change from rho-dependent contractility to CDC-dependent contractility.

(B) Relaxation of pseudo-cleavage is a marker for this transition (so is onset of centration).

(C) CDC-42 also involved in biochemistry (complexing with PAR-6/PKC-3 to inhibit pPARs), so biochemistry and contractility are intimately coupled in maintenance phase (different from establishment phase where rho has its own pulsatile/oscillatory dynamics).

# 2    The steady state of maintenance phase

It has been previously observed that embryos in late-maintenance phase exhibit a steady pattern of anterior-directed cortical flow (see [23, Fig. 2]). Yet, despite the anterior-directed contractility, the A/P boundary in late maintenance appears to be stable. It remains unclear if this pattern of flow is a consequence of establishment-phase patterning of myosin [21], or if the pattern of flow is merely transient and would eventually stop if the cell cycle extended long enough. In this section, we establish that the pattern of flow and myosin profile in maintenance phase are in fact robust and long-lasting; in other words, we seek to show that maintenance-phase biochemistry encodes an attractive steady state.

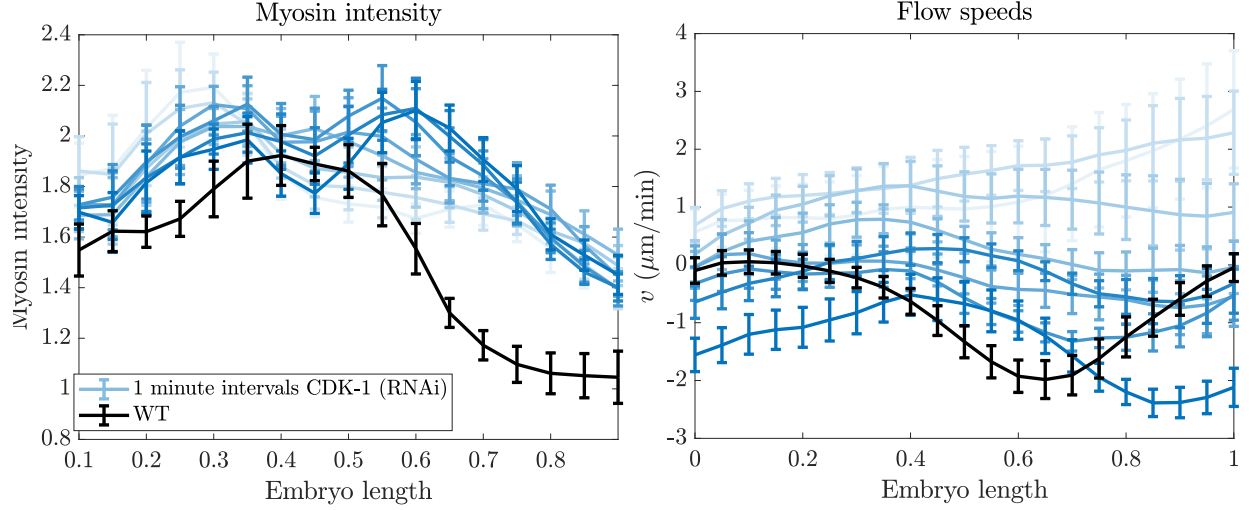## 2.1    Maintenance-phase rescue

In addition to stabilizing asymmetries that are set up during establishment phase, the biochemical and mechanical interactions in maintenance phase can also rescue a steady polarized state. While
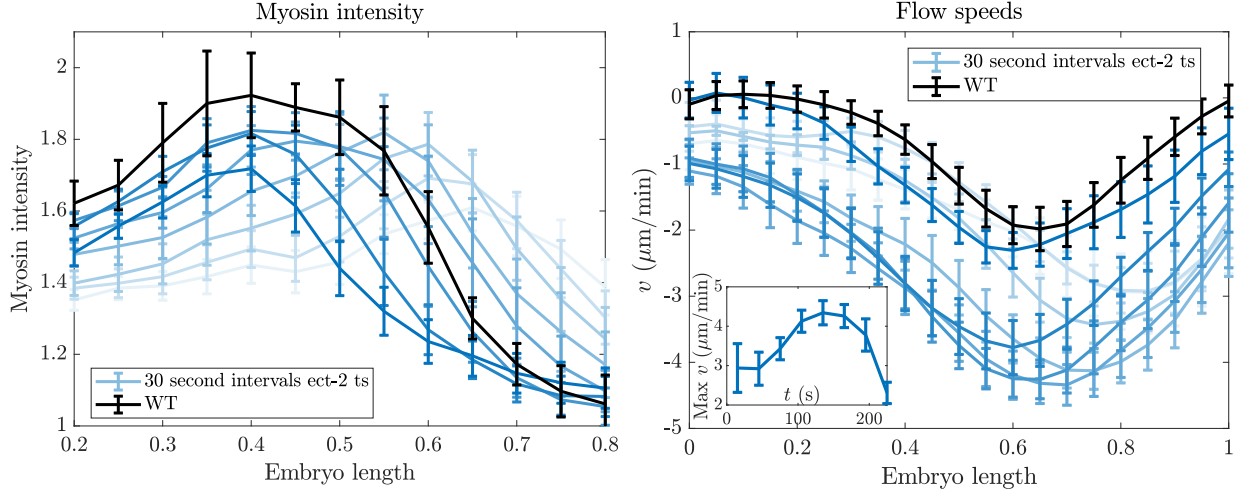
**Figure 1:** Comparing the end of maintenance phase in *ts ect-2* mutants to wild-type embryos. Left panel: myosin intensity profile. Right panel: flow speeds (inset shows the maximum flow speed over time). The blue colored lines show 30-second intervals of maintenance phase in *ts ect-2* embryos, with darker blue denoting later times. The black line shows the profile extracted from the last minute of maintenance phase in wild type embryos [23].

this has been observed in previous studies in *ect-2* mutants [27, 26], which lack Rho functionality during establishment phase, it has yet to be shown that the steady polarized state that results is the same as in wild-type embryos. To establish this, we systematically image rescue of symmetry breaking in temperature-sensitive *ect-2* mutants, marking the beginning of maintenance phase via the transition of myosin from large to small clusters, and the end of maintenance phase as the onset of embryo rotation prior to cytokinesis. This gives a roughly four minute window of maintenance phase for each embryo, in which we track the average myosin intensity profile and flow speed.

In the SI, we plot the myosin intensity profile and flow speed as a function of time by looking at the average over each minute of maintenance phase. In minutes 1–3 of maintenance phase, the myosin boundary shifts to the left, and the flow speed increases. In minute 4, the boundary appears to be roughly pinned, and we see a corresponding decrease in the flow speed towards the typical value (2 $\mu$m/min) observed in wild-type embryos. To establish the comparison more clearly, in Fig. 1 we show the myosin intensity and flow speed over 30 second intervals, and compare the result to the steady myosin intensities and flow speeds observed in wild-type embryos [23]. There we a myosin peak which initially advances rapidly, and is subsequently pinned at about 40% embryo length. The pinning of the myosin peak corresponds to a decrease in the maximum flow speed from about 4.5 $\mu$m/min to 2 $\mu$m/min in the last 30 seconds of maintenance phase (see the inset

**Figure 2:** Comparing the end of maintenance phase in *CDK-1* (RNAi) mutants to wild-type embryos. Left panel: myosin intensity profile. Right panel: flow speeds. The blue colored lines show 1-minute intervals of maintenance phase in *CDK-1* (RNAi) embryos, with darker blue denoting later times. The black line shows the profile extracted from the last minute of maintenance phase in wild type embryos [23].

of Fig. 1). In the last 30 seconds of maintenance phase, the flow profile in *ts ect-2* embryos is roughly the same as that observed during late maintenance phase in wild-type embryos. The myosin intensity appears quantitatively different, but has the same fundamental shape: there is a gradient of myosin in both the anterior and posterior, with a maximum occurring at around 40% of the embryo length. These results establish that the biochemical circuit governing maintenance phase can amplify small residual asymmetries from establishment phase, and that the resulting polarized state is independent of what comes before maintenance.

### 2.1.1 Rescue requires MRCK

## 2.2 Persistent pattern of cortical flow

The pinning of the myosin boundary and subsequent decrease in the speed of flow hint that the cell has a built-in mechanism to prevent the boundary from contracting off the end of the embryo. But is it really possible to maintain a steady myosin intensity profile in the presence of a persistently anterior-directed flow?

To probe whether the myosin intensity and patterns of flow we see in late maintenance phase are truly steady states, we extend maintenance phase by treating wild-type embryos with CDK-1 (RNAi). Marking the start of maintenance phase by the end of pseudo-cleavage, and the end of

maintenance phase by the onset of cytokinesis, we obtain a window of roughly 8–10 minutes per cell, in which we characterize the myosin intensity and flow speeds. The SI shows the profiles of individual embryos and the mean over a succession of eight minutes that culminate at the end of maintenance in each embryo. We collect these data in Fig. 2, where we plot the progression of maintenance phase with darker lines. In wild-type embryos, the start of maintenance is characterized by a posterior-directed flow, and this is observed in *CDK-1* (RNAi) embryos as well (lightest lines in Fig. 2). Later stages of maintenance show a relatively stable position of the myosin boundary (it in fact expands towards the posterior slightly) and a persistent anterior-directed flow which tends to achieve a maximum (magnitude) just posterior of the peak myosin location. While these data do not establish that the exact myosin and flow profiles are true steady states, they clearly demonstrate that the embryos can maintain the myosin boundary position, even in the presence of a persistent anterior-directed flow.

# 3  Model reveals existing mechanisms cannot explain rescue

Our goal in this section is to explore existing literature mechanisms for how maintenance phase biochemistry could set an attractive steady state. At first glance, it appears that the phenomenon of maintenance phase rescue is a consequence of an instability of the underlying system; a small perturbation in the myosin concentration could induce an anterior-directed flow, which drives the system to the polarized state. Here we systematically exclude this by considering a model of myosin alone and showing that spontaneous symmetry breaking is not possible with realistic parameters. We then consider PAR proteins, showing that, while the PAR circuit we consider can maintain a stable polarized state with a fixed boundary position, the time required to set up this state is prohibitively long, and myosin-directed flows are required. Finally, we consider a combination of myosin-driven flows *and* PAR proteins. This model allows us to reproduce the initial stages of maintenance phase rescue, but it cannot explain the sudden slow-down in flow speeds and pinning of the myosin boundary.

## 3.1  Myosin without additional feedback cannot spontaneously polarize

We first explore the dynamics of myosin alone, which we describe in terms of a one-dimensional spatially and temporally varying field $M(x,t)$ which evolves according to the advection-diffusion-
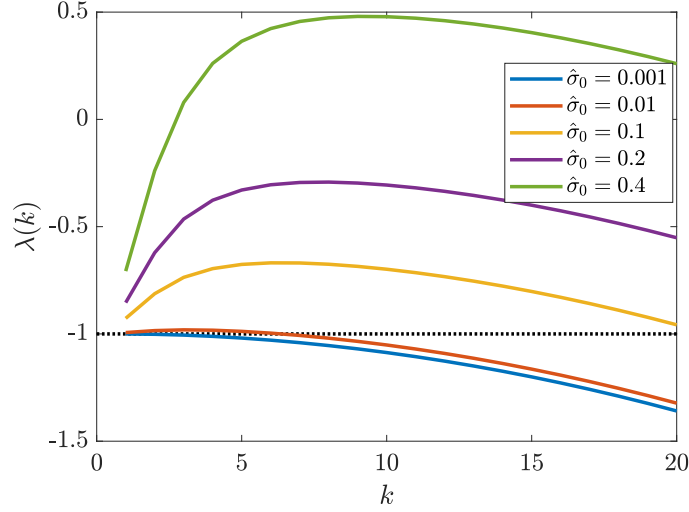
**Figure 3:** Stability analysis for myosin model (1). We consider perturbations of size proportional to $e^{\lambda(k)\hat{t}+2\pi ik\hat{x}}$, then solve the linearized form of (1) to obtain $\lambda(k)$ (see SI). This plot shows $\lambda(k)$ as a function of $k$ and $\hat{\sigma}_0$ (the dimensionless velocity). Positive eigenvalues indicate instability of the steady state. Dotted black line at $\lambda = -1$ reflects the axis of instability *without* unbinding kinetics.

reaction equations [2]

$$\partial_t M + \partial_x(vM) = D_M \partial_x^2 M + k_M^{\text{on}} M_{\text{cyto}} - k_M^{\text{off}} M \tag{1a}$$

$$\gamma v = \eta \partial_x^2 v + \partial_x \sigma_a(M) \tag{1b}$$

$$M_{\text{cyto}} = \frac{1}{hL}\left(M^{(\text{Tot})}L - \int_0^L M(x)\,dx\right) \tag{1c}$$

The velocity field (1b) comes from the assumption that myosin generates an active stress $\sigma_a(M)$, which combines with the viscous stress to give the total cortical stress $\sigma = \eta\partial_x v + \sigma_a(M)$. As in [2], we ignore the elastic part of the stress, since the actomyosin cortex is purely viscous on timescales longer than the cortical turnover time [19]. The force balance equation in the fluid says that the force due to stress must be balanced by the drag force, $\gamma v = \partial_x \sigma$, where $\gamma$ is the drag coefficient. Combining the force balance with the stress expression gives the velocity equation (1b).

In the supplemental text, we non-dimensionalize the model equations (1) and reduce the stability analysis to a single dimensionless group $\hat{\sigma}_0 = \bar{v}/(Lk_M^{\text{off}})$. As $\bar{v}$ represents the typical velocity scale, $1/k_M^{\text{off}}$ the time a myosin molecule is bound to the cortex, and $L$ the embryo perimeter, the dimensionless parameter $\hat{\sigma}_0$ describes the fraction of the embryo perimeter over which a myosin molecule is transported in the time it sits on the cortex.

To analyze stability, we introduce a perturbation around the uniform steady state of myosin,

8
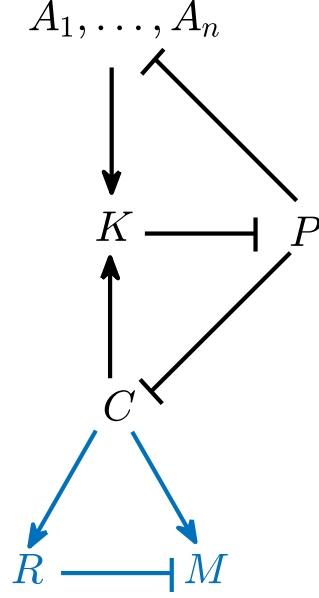
**Figure 4:** Schematic of the biochemistry model. We consider the black parts (biochemistry only) in Section 3.2, and add the blue parts (contractility) in Section 3.4. On the anterior half, $A$ represents PAR-3 (in monomer and oligomer form), $K$ represents the PAR-6/PKC-3 complex, and $C$ represents CDC-42. The posterior PARs can be represented by a single protein species $P$.

$\hat{M} = \hat{M}_0 + \delta\hat{M}$, where $\delta\hat{M} = \delta\hat{M}_0 e^{\lambda(k)\hat{t}+2\pi ik\hat{x}}$, and linearize (1) to solve for the eigenvalue $\lambda(k)$ (see supplemental text; positive eigenvalues mean growth of the perturbation and instability, negative eigenvalues mean decay of the perturbation and stability). Figure 3 shows the value of $\lambda(k)$ as a function of wavelength $k$ and dimensionless flow speed $\hat{\sigma}_0$. We observe strong flow coupling required for instability; with $\hat{\sigma}_0 = 0.2$ (flow transports myosins around 20% of the cell before they come off), we still do not see any instability. In wild-type embryos, we estimate $\hat{\sigma}_0 \approx 0.04$ (see SI), and thus myosin cannot self-polarize in the zygote. As discussed in the SI, in maintenance phase embryos, the main factor working against build-up of myosin is the short residence time (about 10 s). Specifically, the advective flow must be strong enough to overcome the local increase in unbinding that happens in areas enriched in myosin. Our data clearly demonstrate that this does not occur in maintenance phase, making the dynamics of myosin by itself stable to perturbations. This means that maintenance-phase rescue must be a result of PAR proteins signaling myosin. The next section lays out our model of the maintenance phase PAR protein circuit that we use for this purpose.

## 3.2  Basic maintenance-phase biochemistry circuit

Our biochemistry model is based on the diagram shown in Fig. 4, which in turn comes from [17, Fig. 2]. On the anterior side, we have three distinct protein species: PAR-3 ($A$), CDC-42 ($C$), and PAR-6/PKC-3 ($K$), each of which has a separate function. The posterior PARs (PAR-2, PAR-1, and CHIN-1) can be lumped into one species (denoted by $P$), which antagonizes both PAR-3 and CDC-42. The dimensional equations which describe the circuit are

$$\partial_t A_1 = D_A \partial_x^2 A_1 + \left(k_A^{\mathrm{on}} + k_A^+ f_A^+(A)\right) A_{\mathrm{cyto}} - k_A^{\mathrm{off}} A_1 \tag{2a}$$

$$+ 2k_A^{\mathrm{dp}}(P)\hat{A}_2 - 2k_A^{\mathrm{p}}\hat{A}_1^{\,2} + \sum_{n=3}^{N}\left(A_n - k_A^{\mathrm{dp}}(P)A_1 A_{n-1}\right)$$

$$\partial_t A_n = k_A^{\mathrm{p}} A_1(A_{n-1} - A_n) - k_A^{\mathrm{dp}}(P)(A_n - A_{n+1}) \qquad N > n \geq 2 \tag{2b}$$

$$\partial_t A_N = k_A^{\mathrm{p}} A_1 A_{N-1} - k_A^{\mathrm{dp}}(P)A_N \tag{2c}$$

$$\partial_t C = D_C \partial_x^2 C + k_C^{\mathrm{on}} C_{\mathrm{cyto}} - k_C^{\mathrm{off}}\left(1 + r_{\mathrm{PC}}P\right)C \tag{2d}$$

$$\partial_t K = D_K \partial_x^2 K + r_{\mathrm{ACK}} C \delta_{A>A_0} K_{\mathrm{cyto}} - k_K^{\mathrm{off}} K \tag{2e}$$

$$\partial_t P = D_P \partial_x^2 P + k_P^{\mathrm{on}} P_{\mathrm{cyto}} - k_P^{\mathrm{off}}\left(1 + \hat{r}_{\mathrm{KP}}K\right)P \tag{2f}$$

The PAR-3 equations (3a)–(3c) describe the dynamics of PAR-3 oligomerization (an oligomer of size $n$ denoted by $A_n$), for which we use the model developed in [16]. As discussed in detail there, the combination of oligomerization and positive feedback (through the term $k_A^+ f_A^+(A)$) imparts intrinsic bistability to the system. This bistability is strengthened when pPARs are included; through the term $k_A^{\mathrm{dp}}(P)$, these posterior PARs promote depolymerization of PAR-3.

PAR-3 also gates the association of CDC-42 with PAR-6/PKC-3 ($K$), which is a complex that inhibits all posterior PARs. To model this, we work off the observations in [23], which reveal that PAR-6/PKC-3 are recruited to the membrane by CDC-42, provided that there is a sufficient concentration (roughly 10% of the enriched anterior level) of PAR-3 on the membrane. Thus the total loading term in (3e) is proportional to the CDC-42 concentration times the cytoplasmic concentration of $K$, provided the PAR-3 concentration satisfies $A > A_0$. The other two equations (for CDC-42 and pPARs) are straightforward: we assume a basal rate of binding and unbinding, with an unbinding rate which is linearly enhanced by the inhibitor (pPARs for CDC-42 and PKC-3 for pPARs). In the supplemental appendix, we nondimensionalize (2), then use sets of existing experimental observations about the relative amount of each species on the anterior/posterior side of the embryo, as well as estimates of the amounts in the cortex vs. cytoplasm, to constrain all of

the unknown parameters.

## 3.3   PAR proteins without contractility amplify asymmetries, but too slowly

In previous work on PAR-3 [16], we demonstrated that the diffusion of the smaller oligomer sizes (monomers in our model) sets a unique boundary position. Because the shift in the boundary is controlled by the slow process of diffusion, it occurs on timescales of hours, meaning that the boundary never reaches a steady position in practice. In Fig. 5, we demonstrate that this observation still holds when we account for the full biochemistry. In particular, we show the contraction of a PAR-3 domain that initially takes up 90% of the embryo (pPARs are enriched in the other 10%). Initially, the boundary shifts because a high concentration of pPARs shifts the local equilibrium of PAR-3 oligomerization towards the monomer state, which makes bistability impossible [16]. Consequently, we observe contraction of the PAR-3 domain, with a peak that grows over time, and expansion of the PAR-2 domain, both of which eventually reach a steady state.

The concentration of PAR-2 at the edge of the domain decreases over time, which suggests that cytoplasmic depletion might be responsible for halting the boundary, as there is at some point too much $A$ and not enough $P$ for $P$ to win the competition. To demonstrate that a fixed pool of protein is key to arresting posterior domain expansion, in the right panel of Fig. 5 we simulate with a cytoplasmic pool that is "frozen" at its value at $t = 10$ mins. The result is an anterior domain which shrinks at a constant rate with constant peak concentration, and a posterior domain which expands at a constant rate with the same concentration at the edge. Given enough time (2 hours in this case), the posterior domain invades the entire embryo length.

As shown in Fig. 6, cytoplasmic depletion can indeed pin the aPAR/pPAR boundary at a unique position, but the timescales involved (hours) are much slower than the total timescale of maintenance phase (at most 5 minutes). If we begin with 90% PAR-3 enrichment, Fig. 6 shows that the PAR-3 domain size shrinks to roughly 80% after 5 minutes of real time. That said, if we were to start at 50% PAR-3 enrichment, the march to steady state appears much faster (about 5 minutes). In order to reproduce rescue, we need to introduce cortical flows that shift the boundary at a faster initial rate.

## 3.4   Coupling contractility to biochemistry reproduces initial stages of rescue

Because myosin cannot form patterns on its own, there must be an interaction with PAR proteins that amplifies gradients in contractility to rescue the correct polarized state. To account for this,
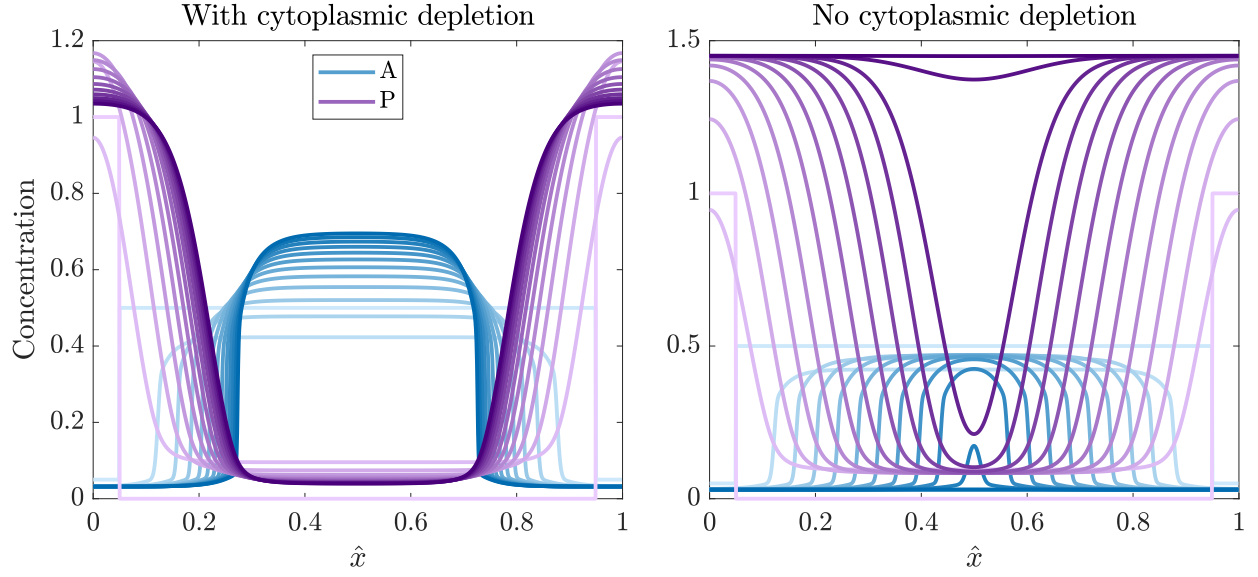
**Figure 5:** Simulating the biochemistry dynamics (2) with (left) and without (right) cytoplasmic depletion. We show a sequence of 13 time points from $t = 0$ (the lightest colors) to $\hat{t} = 120$ mins (the darkest colors). The left plot shows results with the equations as written, while the right plot removes the cytoplasmic pool updates after $t = 10$ mins. For clarity of the plot, we show only PAR-3 in blue and pPARs in purple.
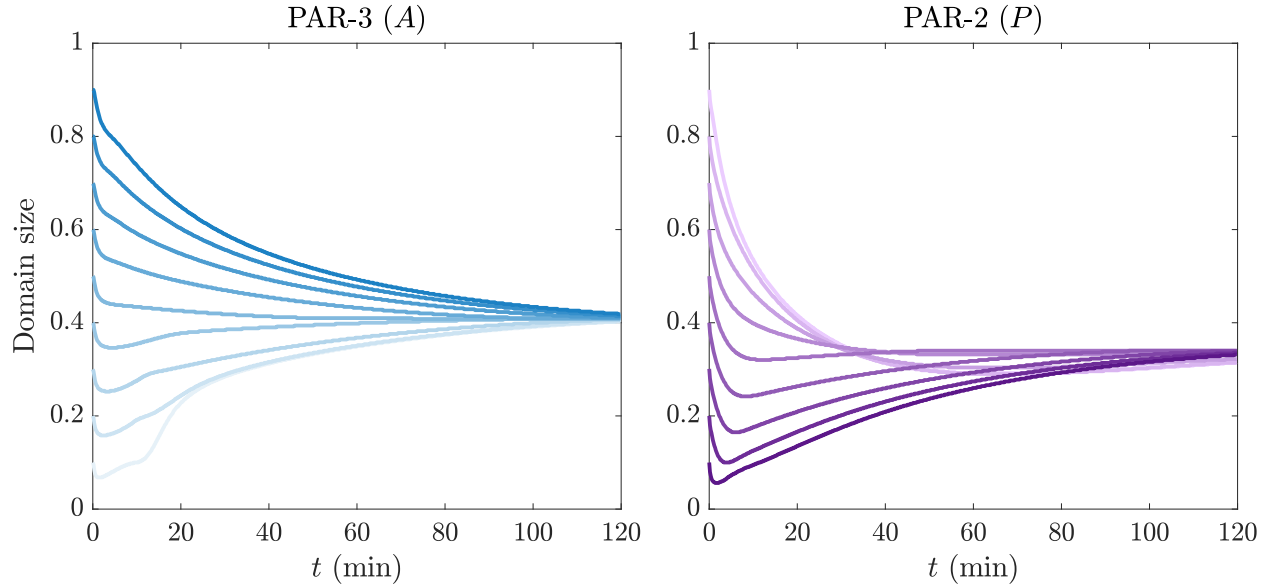


**Figure 6:** Size of the PAR-3 (left) and PAR-2 (right) domain over time for simulations of the model (2). Here the domain size is measured by the length of domain where a particular protein concentration is 80% of its maximum or larger. Darker lines here denote domain sizes that are initially larger in PAR-3 (corresponding to the realistic situation).

we add the myosin dynamics (1) to the biochemistry system (2). In doing this, we also incorporate advective terms that ensure that each protein moves with the local cortical velocity [13], and make CDC-42 a promoter of myosin by adding a term of the form $r_{\mathrm{CM}}CM_{\mathrm{cyto}}$. The dimensional equations corresponding to this situation are

$$\partial_t A_1 + \partial_x (vA_1) = D_A \partial_x^2 A_1 + \left( k_A^{\mathrm{on}} + k_A^+ f_A^+(A) \right) A_{\mathrm{cyto}} - k_A^{\mathrm{off}} A_1 \tag{3a}$$

$$+ 2k_A^{\mathrm{dp}}(P)\hat{A}_2 - 2k_A^{\mathrm{p}}\hat{A}_1^{\,2} + \sum_{n=3}^{N} \left( A_n - k_A^{\mathrm{dp}}(P)A_1 A_{n-1} \right)$$

$$\partial_t A_n + \partial_x (vA_n) = k_A^{\mathrm{p}} A_1 (A_{n-1} - A_n) - k_A^{\mathrm{dp}}(P)(A_n - A_{n+1}) \qquad N > n \geq 2 \tag{3b}$$

$$\partial_t A_N + \partial_x (vA_N) = k_A^{\mathrm{p}} A_1 A_{N-1} - k_A^{\mathrm{dp}}(P)A_N \tag{3c}$$

$$\partial_t C + \partial_x (vC) = D_C \partial_x^2 C + k_C^{\mathrm{on}} C_{\mathrm{cyto}} - k_C^{\mathrm{off}} \left( 1 + r_{\mathrm{PC}}P \right) C \tag{3d}$$

$$\partial_t K + \partial_x (vK) = D_K \partial_x^2 K + r_{\mathrm{ACK}}C\delta_{A>A_0} K_{\mathrm{cyto}} - k_K^{\mathrm{off}} K \tag{3e}$$

$$\partial_t P + \partial_x (vP) = D_P \partial_x^2 P + k_P^{\mathrm{on}} P_{\mathrm{cyto}} - k_P^{\mathrm{off}} \left( 1 + \hat{r}_{\mathrm{KP}}K \right) P \tag{3f}$$

$$\partial_t M + \partial_x (vM) = D_M \partial_x^2 M + (k_M^{\mathrm{on}} + r_{\mathrm{CM}}C) M_{\mathrm{cyto}} - k_M^{\mathrm{off}} M \tag{3g}$$

$$\gamma v = \eta \partial_x^2 v + \partial_x \sigma_a(M). \tag{3h}$$

In the SI, we non-dimensionalize this system of equations and use existing data to obtain some the unknown parameters, finding that one parameter is completely unknown: $\hat{R}_{\mathrm{CM}} = r_{\mathrm{CM}}C^{(\mathrm{Tot})}/k_M^{\mathrm{on}}$. This parameter defines the strength at which CDC-42 promotes binding of myosin, relative to the basal rate. In Fig. 7, we simulate the maintenance phase rescue process, choosing the parameter $\hat{R}_{\mathrm{CM}} = 10$ to match the initial speed of rescue. The left panel shows the dynamics of the simulation from $t = 0$ (lightest colors) to $t = 7.5$ mins (darkest colors), while the right panel shows the myosin boundary position (0 is the anterior pole, 1 is the posterior pole) and the flow speeds over time. Here we plot the region of time where there is a noticeable myosin asymmetry (some part of the domain has a concentration that is half of the maximum).

Our statistics show the beginning of the rescue process, where an initially peaked profile of PAR-2 invades the anterior domain, concentrating anterior PARs in the middle and thereby increasing the concentration of pPARs in the posterior. As a result of this, CDC-42 gets inhibited in the posterior, which gives a gradient of myosin from posterior to anterior. The gradient of myosin generates a flow which further compacts the anterior domain. The timescale of this compaction is much faster than without flows (Fig. 6), and indeed occurs on a timescale of minutes and not hours.
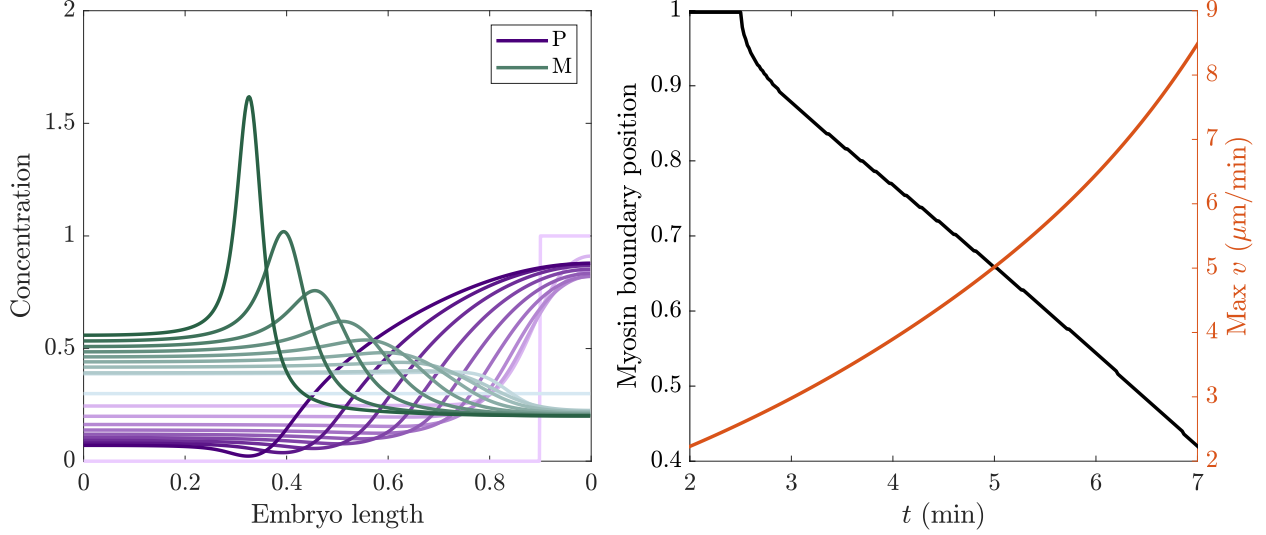
**Figure 7:** Attempting to reproduce maintenance-phase rescue using the model (3). Left panel: time course of rescue, with lines shown at equal time points from $t = 0$ to $t = 7.5$ mins (intervals of 45 seconds). The blue lines, purple, and green lines show PAR-3 ($A$), pPARs ($P$), and myosin ($M$), respectively. Right panel: the position of the myosin boundary (defined as the point where myosin exceeds half-max, where 0 is the anterior pole and 1 is the anterior pole) over time (black curve, left axis) and the corresponding flow speed (red curve, right axis).

While our model reproduces the initial stages of the rescue process, there is no mechanism in it to halt the advancing myosin front. With the correct model parameters, the concentration of anterior PARs by flow overwhelms the effect of cytoplasmic depletion (which tends to slow the boundary motion). As a result, the boundary contracts with nothing to slow it down. Indeed, in the limit as time goes to infinity, we expect one peak of aPARs and myosin at the anterior pole, which is in sharp contrast to our experimental result which showed a sharp drop in the anterior-directed flow speed in the late stages of maintenance phase (see inset of Fig. 1).

## 4 Branched actin as a brake on contractility

Our modeling so far identified two regimes of behavior, depending on the sensitivity of myosin to the CDC-42 concentration. Roughly speaking, if CDC-42 promotes myosin at a rate much smaller than the basal rate (0 in Fig. 5), the cytoplasmic dynamics are sufficient to stop the pPARs from invading too far into the anterior domain. But this model has to be discarded because the dynamics occur over unrealistically long timescales. To match the speed of rescue, CDC-42 has to promote myosin at a rate much larger than the basal rate, which leads to fast flows and (in this model) a

14
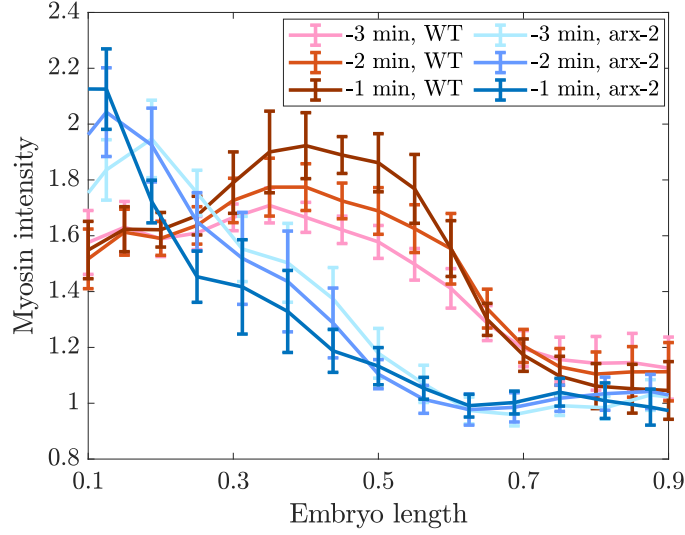
**Figure 8:** Myosin intensity profiles late maintenance phase in wild-type (red lines) and arx-2 (RNAi) treated embryos (blue lines). The lightest colors show the average profile between 2 and 3 minutes prior to cytokinesis onset, the middle colors between 1 and 2 minutes, and the darkest colors show the profile in the last minute of maintenance phase.

rapid concentration of the anterior domain into a peaked profile at the anterior pole. Thus, we are missing an important interaction that slows down the advancing myosin peak, and rapidly drops the flow speed. This interaction is the focus of this section.

## 4.1 Experiments in arx-2 (RNAi) embryos establish hyper-contractile state

We hypothesize that branched actin might stop the anterior cap from becoming hyper-contractile. To test this hypothesis, we deplete wild type embryos of arx-2, a protein which activates the arp 2/3 complex and the assembly of branched actin. Figure 8 shows the average myosin intensity profiles over the last three minutes of maintenance phase in wild-type (red) and arx-2 (RNAi) treated embryos (blue). While the wild-type intensity seems to be roughly stalled at a boundary position 40% of the embryo length, the arx-2 (RNAi) embryos demonstrate hyper-contractility, with a myosin intensity that only grows in time near the anterior boundary. The corresponding flow measurements are chaotic and noisy, so we do not show them here. These data clearly establish, however, that the qualitative behavior in embryos *without* branched actin matches what our previous model might have predicted (a hyper-contractile state). In other words, it is the lack of branched actin inhibiting contractility in our model that makes it fail to reproduce the correct rescue dynamics.

## 4.2 Model of branched actin

To model branched actin, we work off the following two important observations from our maintenance-phase rescue experiments:

1. The pinning of the myosin domain and drop in velocity happens quite abruptly (Fig. 1).

2. The rapid drop in velocity is *not* accompanied by strong changes in the myosin concentration profile (Fig. 1).

These observations together suggest that there is an ultra-sensitive dependence of contractility (not myosin concentration) on branched actin. As rescue progresses, branched actin becomes concentrated on the anterior, locally becoming more dense, and activating the braking process.

To incorporate branched actin into our modeling framework, we propose a simple advection-reaction equation, where branched actin is created at a rate proportional to the local membrane-bound CDC-42 concentration, and unbinds with characteristic frequency (about $1/10$ s$^{-1}$)

$$\partial_t R + \partial_x(vR) = r_{\text{CR}} C R_{\text{cyto}} - k_R^{\text{off}} R. \tag{4}$$

In our model, the ultra-sensitivity comes in the contractile response to branched actin. We introduce a scaled variable $\Delta R = \max\left((R - R_c)/\delta_R, 0\right)$, which is zero below a threshold $R_c$ and grows linearly with increasing $R$ after exceeding the threshold. We then propose two possible mechanisms for the ultra-sensitivity
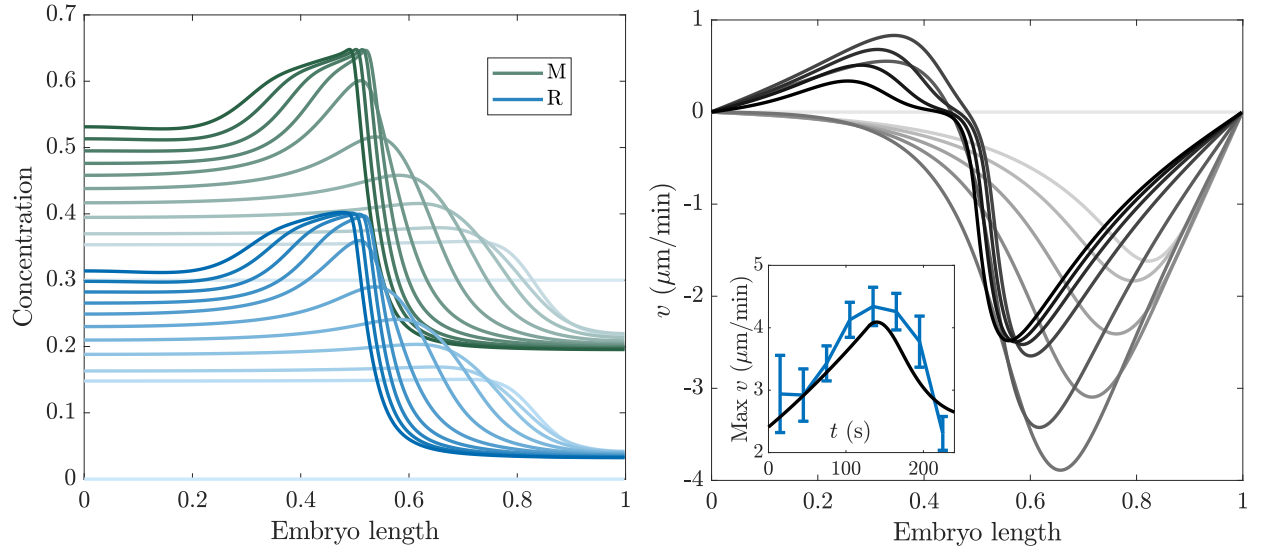
1. Branched actin inhibits the ability of myosin to generate stress. We implement this by modifying the stress (1b) to become ultra-sensitive to branched actin, $\sigma_a = \sigma_0 M e^{-\Delta R}$. Thus, as the branched actin concentration increases above the threshold, the stress exerted by myosin goes rapidly to zero. In this model, branched actin does not impact the response to stress, but the ability to generate it.

2. Branched actin increases the drag coefficient of the surrounding medium. We implement this by modifying the drag coefficient $\gamma$ in (1b) to become ultra-sensitive to branched actin, $\gamma = \gamma_0 e^{\Delta R}$, so that drag becomes infinite as branched actin goes above the threshold. In this model, myosin can generate the same amount of stress, but it cannot propagate to other regions of the embryo because of the high drag coefficient.

Figure 9 shows simulations of the maintenance-phase rescue with these two models of branched actin. In both cases, the myosin boundary initially advances, branched actin sits everywhere below
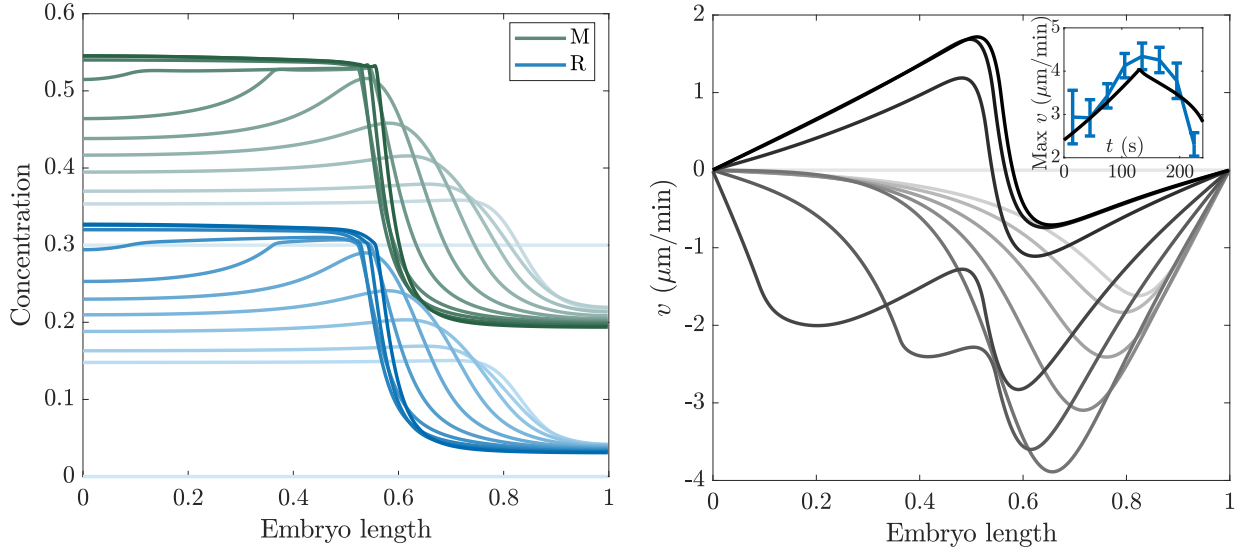
(a) Model 1: Branched actin inhibiting stress



(b) Model 2: Branched actin increasing drag

**Figure 9:** Models for how branched actin inhibits contractility and pins the boundary. Left panel: trajectory of myosin (green) and branched actin (blue) over a 10 minute simulation of maintenance phase rescue (snapshots are show every minute). Right panel: trajectory of velocity $v$. Inset: the maximum anterior-directed flow over time, with time 0 at 3 minutes of simulation time (when the simulated velocity profile approximately matches the first detected experimental profile). Both models contain an ultra-sensitive dependence of velocity on branched actin, but (a) works through the stress $\sigma_a$, while (b) works through the drag coefficient $\gamma$.

the threshold (set to 0.3 here) required for activation of the response. Once branched actin gets sufficiently concentrated, the inhibition of contractility is sufficient to slow and eventually stop boundary progression (by cytoplasmic depletion).

The interesting distinction between the two models lies in the flow patterns that they predict. In the model where branched actin inhibits stress, there is initially a local inhibition of stress at the myosin peak. This leads to a weakening of the flow there, and an intermediate flow profile which has two local minima, separated by the point of weakened stress (right panel of Fig. 9(a)). The weakened stress in the middle of the embryo accentuates the gradient at the anterior end, and the velocity at the anterior increases in magnitude, causing the levels of myosin and branched actin at the embryo end to level out. This further inhibits stress, which then reverses the direction of flow, so that the steady state flow profile has a large positive component in the anterior end.

In the model with higher drag coefficient, the effect of branched actin assembly is to create a "wall" that drops the hydrodynamic lengthscale and prevents the stress gradients from generating large-scale flows. As a result of this, there is a persistent peak in myosin at the embryo midpoint (although there is slow growth in the anterior coming from enrichment of CDC-42 there). The high concentration of branched actin in the anterior prevents the anterior gradient of myosin from generating a large velocity, while the posterior gradient is still able to do so. The steady flow profile therefore has little activity in the anterior, followed by a drop in the posterior.

The key factors which distinguish the drag coefficient model from the stress inhibition model are the peak in myosin in the embryo interior, and the steady flow profile. Both of these match our experimental data for rescue, and so we believe this to be the correct model for how branched actin inhibits contractility. In wild-type embryos that are fixed in maintenance phase and stained with phalloidin (Fig. 2 Ed's paper draft) there seems to be a gradient in branched actin from the anterior pole to the anterior cap, followed by a sharp drop off in the posterior. *wsp-1* (RNAi) reveals that the anterior cap is comprised of a wall of "mini comets," which are dense patches of branched actin. We believe that these dense patches could exponentially increase the drag coefficient on the cortex (in other words, exponentially increase the force required to move them the same velocity).

## 5   Discussion

There is still a role for cytoplasmic depletion in pinning the boundary. Without cytoplasmic depletion, a boundary that is moving will always keep moving, since the fundamental balance

in which pPARs outcompete the aPARs does not change unless we account for changes in the cytoplasmic depletion. What branched actin allows for is a change in how the flow speed depends on the myosin concentration in time. Initially, when there is no branched actin, flows are fast. But, when branched actin is created, the flows slow down and the boundary can no longer rapidly contract, allowing it to be stalled by cytoplasmic depletion. Thus, branched actin *and* cytoplasmic depletion work together to stall the boundary at a point where the posterior PAR domain can no longer advance through the anterior PARs.

# References

[1] Alexander Beatty, Diane G Morton, and Kenneth Kemphues. Par-2, lgl-1 and the cdc-42 gap chin-1 act in distinct pathways to maintain polarity in the c. elegans embryo. *Development*, 140(9):2005–2014, 2013.

[2] Justin S Bois, Frank Jülicher, and Stephan W Grill. Pattern formation in active fluids. *Biophysical Journal*, 100(3):445a, 2011.

[3] Adrian A Cuenca, Aaron Schetter, Donato Aceto, Kenneth Kemphues, and Geraldine Seydoux. Polarization of the c. elegans zygote proceeds via distinct establishment and maintenance phases. 2003.

[4] Adriana T Dawes and David Iron. Cortical geometry may influence placement of interface between par protein domains in early caenorhabditis elegans embryos. *Journal of theoretical biology*, 333:27–37, 2013.

[5] Adriana T Dawes and Edwin M Munro. Par-3 oligomerization may provide an actin-independent mechanism to maintain distinct par protein domains in the early caenorhabditis elegans embryo. *Biophysical journal*, 101(6):1412–1422, 2011.

[6] Evan B Dewey, Danielle T Taylor, and Christopher A Johnston. Cell fate decision making through oriented cell division. *Journal of developmental biology*, 3(4):129–157, 2015.

[7] Wan Jun Gan and Fumio Motegi. Mechanochemical control of symmetry breaking in the caenorhabditis elegans zygote. *Frontiers in Cell and Developmental Biology*, 8:619869, 2021.

[8] Raphaela Geßele, Jacob Halatek, Laeschkir Würthner, and Erwin Frey. Geometric cues stabilise long-axis polarisation of par protein patterns in c. elegans. *Nature communications*, 11(1):539, 2020.

[9] Nathan W Goehring, Philipp Khuc Trong, Justin S Bois, Debanjan Chowdhury, Ernesto M Nicola, Anthony A Hyman, and Stephan W Grill. Polarization of par proteins by advective triggering of a pattern-forming system. *Science*, 334(6059):1137–1141, 2011.

[10] Bob Goldstein and Ian G Macara. The par proteins: fundamental players in animal cell polarization. *Developmental cell*, 13(5):609–622, 2007.

[11] Peter Gross, K Vijay Kumar, Nathan W Goehring, Justin S Bois, Carsten Hoege, Frank Jülicher, and Stephan W Grill. Guiding self-organized pattern formation in cell polarity establishment. *Nature physics*, 15(3):293–300, 2019.

[12] Niv Ierushalmi and Kinneret Keren. Cytoskeletal symmetry breaking in animal cells. *Current Opinion in Cell Biology*, 72:91–99, 2021.

[13] Rukshala Illukkumbura, Nisha Hirani, Joana Borrego-Pinto, Tom Bland, KangBo Ng, Lars Hubatsch, Jessica McQuade, Robert G Endres, and Nathan W Goehring. Design principles for selective polarization of par proteins by cortical flows. *Journal of Cell Biology*, 222(8), 2023.

[14] Kenneth J Kemphues, James R Priess, Diane G Morton, and Niansheng Cheng. Identification of genes required for cytoplasmic localization in early c. elegans embryos. *Cell*, 52(3):311–320, 1988.

[15] Natalia Kravtsova and Adriana T Dawes. Actomyosin regulation and symmetry breaking in a model of polarization in the early caenorhabditis elegans embryo: symmetry breaking in cell polarization. *Bulletin of mathematical biology*, 76:2426–2448, 2014.

[16] Charles F Lang, Alexander Anneken, and Edwin Munro. Oligomerization and feedback on membrane recruitment stabilize par-3 asymmetries in c. elegans zygotes. *bioRxiv*, pages 2023–08, 2023.

[17] Charles F Lang and Edwin Munro. The par proteins: from molecular circuits to dynamic self-stabilizing cell polarity. *Development*, 144(19):3405–3416, 2017.

[18] Jean-Léon Maître, Hervé Turlier, Rukshala Illukkumbura, Björn Eismann, Ritsuya Niwayama, François Nédélec, and Takashi Hiiragi. Asymmetric division of contractile domains couples cell positioning and fate specification. *Nature*, 536(7616):344–348, 2016.

[19] Mirjam Mayer, Martin Depken, Justin S Bois, Frank Jülicher, and Stephan W Grill. Anisotropies in cortical tension reveal the physical basis of polarizing cortical flows. *Nature*, 467(7315):617–621, 2010.

[20] Yoichiro Mori, Alexandra Jilkine, and Leah Edelstein-Keshet. Wave-pinning and cell polarity from a bistable reaction-diffusion system. *Biophysical journal*, 94(9):3684–3697, 2008.

[21] Edwin Munro, Jeremy Nance, and James R Priess. Cortical flows powered by asymmetrical contraction transport par proteins to establish and maintain anterior-posterior polarity in the early c. elegans embryo. *Developmental cell*, 7(3):413–424, 2004.

[22] Masatoshi Nishikawa, Sundar Ram Naganathan, Frank Jülicher, and Stephan W Grill. Controlling contractile instabilities in the actomyosin cortex. *Elife*, 6:e19595, 2017.

[23] Anne Sailer, Alexander Anneken, Younan Li, Sam Lee, and Edwin Munro. Dynamic opposition of clustered proteins stabilizes cortical polarity in the c. elegans zygote. *Developmental cell*, 35(1):131–142, 2015.

[24] Stephanie Schonegg and Anthony A Hyman. Cdc-42 and rho-1 coordinate acto-myosin contractility and par protein localization during polarity establishment in c. elegans embryos. 2006.

[25] Filipe Tostevin and Martin Howard. Modeling the establishment of par protein polarity in the one-cell c. elegans embryo. *Biophysical journal*, 95(10):4512–4522, 2008.

[26] Yu Chung Tse, Michael Werner, Katrina M Longhini, Jean-Claude Labbe, Bob Goldstein, and Michael Glotzer. Rhoa activation during polarization and cytokinesis of the early caenorhabditis elegans embryo is differentially dependent on nop-1 and cyk-4. *Molecular biology of the cell*, 23(20):4020–4031, 2012.

[27] Seth Zonies, Fumio Motegi, Yingsong Hao, and Geraldine Seydoux. Symmetry breaking and polarization of the c. elegans zygote by the polarity protein par-2. *Development*, 137(10):1669–1677, 2010.